

FLUORESCENCE DIFFUSE OPTICAL TOMOGRAPHIC SYSTEM FOR ARBITRARY SHAPED SMALL ANIMALS

A. Koenig, L. Hervé, J. Boutet, M. Berger, J.M. Dinten, A. Da Silva, P. Peltié, P. Rizo

LETI-CEA MINATEC, 17 rue des martyrs - 38054 Grenoble cedex 9 France

ABSTRACT

This paper presents a method based on fluorescence diffuse optical tomography for reconstructing the fluorescence yield of heterogeneous and arbitrary shaped medium such as small animals. The experimental set-up is presented and the associated reconstruction method making mouse inspection without immersion in optical index matching liquid (Intralipid and ink) possible is detailed. Some phantom experiments have been carried out to characterize this new system and to validate its use for non immersed heterogeneous media and a first experiment on a mouse is presented. These results validate further use of our system for biological studies of small animals.

Index Terms— Fluorescence, fluorescence diffuse optical tomography, reconstruction

1. INTRODUCTION

Functional analyses on small animals, and in particular, the study of tumor growth, are usually performed with high-resolution microtomography (micro-CT) as well as MRI but these equipments are expensive. On the contrary, the near-infrared photon migration modality is envisioned to provide cost effective diagnostic tools since the involved pieces of technology are already developed. Furthermore, near-infrared optical tomography joined to fluorescence tagging allows to access to functional information.

By tagging regions of interest with target-specific fluorescing molecular probes [1][2], and using an appropriate technique of tomography (fluorescence-enhanced diffuse optical tomography or fDOT), we can estimate the three-dimensional locations and geometries of the targeted areas [3][4], such as tumors, and quantify the local concentration of probes hence the biological activity. Its potentiality has been widely demonstrated for applications related to preclinical evaluation of novel drug candidates on small animals [5].

An instrument including a dedicated reconstruction scheme has been developed in our laboratory to conduct fDOT experiments. It works with a continuous laser source and in the trans-illumination geometry, i.e., the laser source scans the bottom side of the studied animals and the outgoing transmitted and fluorescence signals are recorded

at the other side. The system deals with two challenges related with the optical molecular imaging which are the complex shapes and the heterogeneity of the optical properties of the small animals. Contrary to a previous article [6] where the method imposed the use of compression plates to flatten the small animals over the region of interest, here, the complexity of the natural shape of the animal is managed by measuring the external boundary of the animal with a laser triangulation technique and by solving the forward model on a mesh adapted to the geometry with the finite volumes method. The optical heterogeneity is accounted for by first reconstructing an optical attenuation map from the transmitted signal. Then, by using the animal specific model which incorporates consistent boundary effects and optical properties, we reconstruct the 3D fluorescence distribution to infer cancer localization and activity.

This paper will at first make a short presentation of the experimental set up and the associated reconstruction approach. It presents the laser triangulation technique used to infer the animal surface. Then experimental results obtained on phantoms are presented to illustrate the use of this method and a mouse experiment is presented.

2. EXPERIMENTAL SET-UP

The experimental setup (Figure 1) consists of a laser source (690 nm, 26 mW, Powertechnology) mounted on two motorized translation stages and a CCD camera (Hamamatsu Orca AG). The wavelength of the laser was chosen after studying the absorption spectrum of living mice which is minimal between 690 and 800 nm. 690 nm was selected because such lasers are commercially available, compact, and cost effective and can also excite a wide range of near-infrared fluorophores which absorption spectrum varies from 660 nm to 750 nm. In order to avoid auto-fluorescence and camera saturation problems, the system was designed in the trans-illumination geometry, i.e. the laser is placed under the animal and the camera above. Thanks to the motorized stages, the animal is scanned by the laser source which typically describes a regular 10 by 10, 2 mm spaced grid (2 cm x 2 cm field of view) under the examined sample. For each source position, the CCD camera focused onto the upper glass window, records at first the transmitted (excitation) images. Then a Schott high pass RG9 filter is

inserted and the fluorescence (emission) images are stored. The exposure time is adapted for each source position in order to take advantage of the entire dynamic range of the camera, even in highly heterogeneous regions of the animal.

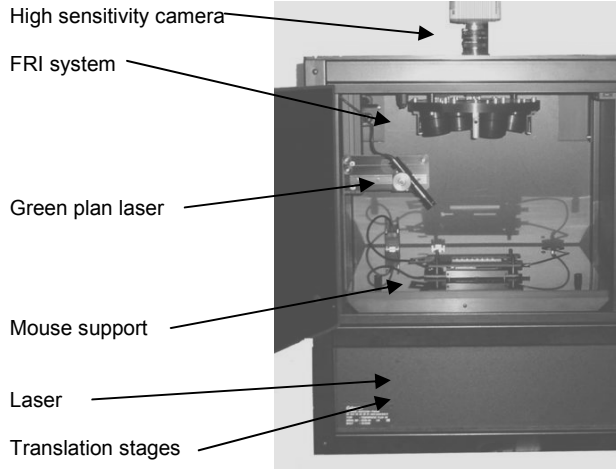


Figure 1: experimental set-up photograph

To work properly, the reconstruction algorithm needs to get information about the surface of the studied medium. To achieve this, it is scanned by an oblique green planar laser (Figure 2) and the intersection curve between the laser plane and the studied object is acquired by the camera.

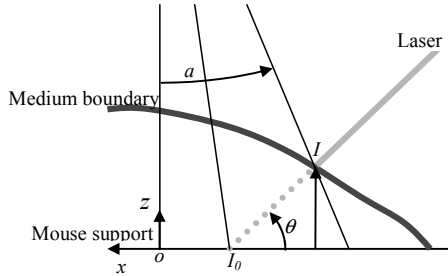


Figure 2: schema of the boundary triangulation

If a is the viewing angle from the camera, θ is the laser angle, I is the intersection of the laser with the medium boundary, I_0 is the intersection of the laser with the support (if there was no medium), H is the distance from support to camera, $x(I)$ is the coordinate of I according to the scanning direction (its origin being taken at the optical axis), $z(I)$ is the height of I , we have :

$$\tan(a(I)).H = (x(I) + \tan(a).z(I)),$$

$$\tan(a(I_0)).H = x(I_0) \text{ and}$$

$$z(I) = \tan(\theta).(x(I) - x(I_0)).$$

Therefore, from any measurement point $(\tan(a(I)), \tan(a(I_0)))$, we can sort out the position of a corresponding surface point $(x(I), z(I))$.

3. RECONSTRUCTION METHOD

3.1. Forward model

Here, the light is modeled as a scalar field $\phi(\mathbf{r})$ and is assumed to follow the Helmholtz equation which is adapted to model the propagation of light in highly diffusive media:

$$\nabla^2 \phi_s(\mathbf{r}) - k(\mathbf{r})\phi_s(\mathbf{r}) = -S_s(\mathbf{r}) \quad (1)$$

where \mathbf{r} is the position in the studied medium, the index s is related to the source position, $k(\mathbf{r})$ is a scalar map called "optical heterogeneity map" and which can be seen as the compound of μ_a (the attenuation coefficient) time μ'_s (the reduced scattering coefficient), and which also takes into account the effects of diffusion variations [7] and the effects of the borders [6].

To complete the description of the system, the extrapolated boundary conditions are used. It states that the field is naught on a surface located at αD farther from the real boundary of the studied object, where α is related to the optical indexes mismatch and D is the diffusion coefficient of the medium. (1) is discretized by using the finite volume method on an unstructured mesh which conforms to the extrapolated boundary and which is determined from the surface provided by the green planar laser illumination. We end up with a linear system $A\Phi=S$ where A is the stiffness matrix, Φ and S are the discretization of the light field and the source on the mesh. This system is solved for each source position (and detector position as we will see below) by using the LU decomposition.

As we are dealing with source points, it is convenient to use the Green functions $G_s(\mathbf{r})$ associated with the system (1):

$$\nabla^2 G_s(\mathbf{r}) - k(\mathbf{r})G_s(\mathbf{r}) = -\delta(\mathbf{r} - \mathbf{r}_s) \quad (2)$$

We have $\phi_s(\mathbf{r}) = \hat{\lambda}.G_s(\mathbf{r})$ with $\hat{\lambda}$ being related to the laser source intensity. So we have the excitation measurement U_{sd}^{ex} taken at a detector position \mathbf{r}_d that follows: $U_{sd}^{ex} = \lambda.G_s(\mathbf{r}_d)$ where λ is related to the laser source intensity and the detection efficiency and has to be calibrated on a reference experiment

3.2. Reconstruction of the optical parameters

As the optical heterogeneity map is highly varying from one organ of a small animal to the other, and is also subject to vary from one animal to the other, it must be reconstructed specifically to the studied medium. This is done by using the Rytov expansion (3a) and (3b) of (1) which states that for "little steps" of variation of k , we have:

$$-G_s(\mathbf{r}_d) \log\left(\frac{U_{sd}^{ex}}{\lambda G_s(\mathbf{r}_d)}\right) = \int_{\Omega} G_s(\mathbf{r}) \Delta k(\mathbf{r}) G_d(\mathbf{r}) d\Omega \quad (3a)$$

Its discretization gives:

$$-G_s(\mathbf{r}_d) \log\left(\frac{U_{sd}^{ex}}{\lambda G_s(\mathbf{r}_d)}\right) = \sum_m G_s(\mathbf{r}_m) \Delta k(\mathbf{r}_m) G_d(\mathbf{r}_m) \Delta V \quad (3b)$$

where Ω is the volume of the studied object, $\Delta k(\mathbf{r}) = k^0(\mathbf{r}) - k(\mathbf{r})$, $k^0(\mathbf{r})$ is the real map of optical heterogeneity we are looking for, $G_d(\mathbf{r})$ is the Green's function associated to (1) for a source located at the detector d position, $\delta(\mathbf{r}-\mathbf{r}_d)$ and ΔV is the elementary voxel volume.

The determination of $k(\mathbf{r})$ is performed from the excitation measurements in an iterative process; at first (step 1), it is initialized with a homogeneous map corresponding to the following optical parameters: $\mu'_s = 10 \text{ cm}^{-1}$, $0.2 < \mu_a < 2 \text{ cm}^{-1}$. μ_a is obtained by fit between the excitation measurements and the forward model. Then (step 2), the Green's functions using the current k map are estimated by solving (2) with the finite volumes method. Finally (step 3), a new k map is reconstructed through an ART (Algebraic reconstruction technique, 5 iterations with a relaxation factor of 0.1) from the current Green functions and Rytov expansion (3b) by comparison to the excitation measurements. Step 2 and 3 are iterated until convergence (15 iterations of the global process are empirically enough to minimize this difference between computed Green's function and observed excitation acquisitions). This process leads to Green's functions which describes the propagation of light in a heterogeneous medium consistently with the excitation measurements.

Once the heterogeneity map is estimated, the fluorescence yield $X(\mathbf{r})$ is reconstructed by solving the discretized form of (4a), i.e. (4b), from emission measurements U_{sd}^{em} using the ART algorithm. Convergence of the algorithm is achieved within 15 iterations and a relaxation factor of 0.1.

$$U_{sd}^{em} = \int_{\Omega} G_s(\mathbf{r}) X(\mathbf{r}) G_d(\mathbf{r}) d\Omega \quad (4a)$$

$$U_{sd}^{em} \approx \sum_m G_s(\mathbf{r}_m) X(\mathbf{r}_m) G_d(\mathbf{r}_m) \Delta V \quad (4b)$$

4. VALIDATIONS

4.1. Validation on a half cylinder phantom

A half cylinder solid phantom described in ref [6] was used to validate the non contact approach developed above (Figure 3 and 4). A fluorescent dot was inserted at a border of the phantom at 1.2 cm above the ground. In this experiment, 10×10 source positions with a 2 mm separation were considered. The CCD camera images of the phantom

were resampled to create 45×45 pixel images covering a $2.2 \times 2.2 \text{ cm}^2$ field of view. A nominal reconstruction mesh composed of 3745 elements with a volume element of $0.2 \times 0.2 \times 0.1 \text{ cm}^3$ was used. Here, the z sampling rate is chosen to be half the x or y since we were interested in studying the z -resolution limit which is known to be the most critical in the transmission geometry.

As detailed above, the surface was scanned with a planar laser and inserted in the description of the direct model of the studied object. The obtained surface is represented in Figure 3 and describes well the phantom geometry (the maximum height is flat and equal to the nominal value (2.5 cm), the width of the phantom is correct).

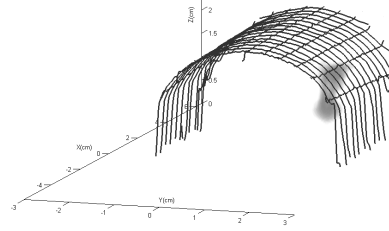


Figure 3: reconstruction of the object surface with the laser triangulation system, and reconstruction of the fluorescence yield.

Then, the optical heterogeneity map and the fluorescence yield were reconstructed using the method presented in section 3.2. The reconstructed fluorescence yield is presented on Figure 4 (and in 3D on figure 3) which shows that the fluorescence tube is correctly reconstructed and is close to the expected position: the lateral position is in the alignment of the syringe head and recovered mean vertical position is found at 1.39 cm. We can also see that, the recovered fluorescence has a vertical dispersion (4.3 mm) much bigger than the lateral one (1.5 mm) in accordance with the fact that the lateral resolution of the system is much better than the vertical resolution.

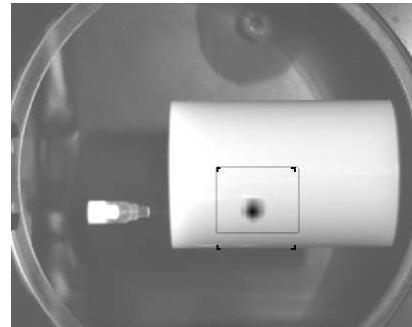


Figure 4: reconstruction of the fluorescence yield of a fluorescent dot inserted inside a half cylinder diffusive phantom.

4.2. Validation on a mouse

We inserted a fluorescent capillary tube (filled with Intralipid and Alexa 750, $20 \mu\text{M}$) in the mouse intestine in

order to validate the reconstruction approach. The mouse was anesthetized and imaged over the abdomen area. Figure 5 shows the reconstruction of the animal boundary over the region of interest.

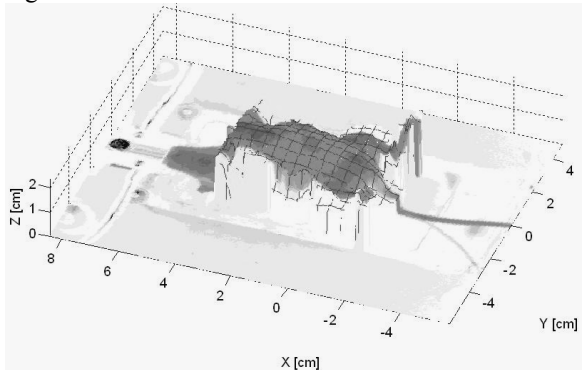


Figure 5: Acquisition over the abdomen area and reconstruction of the mouse surface with the laser triangulation system

The near infra-red laser describes a 10 by 11, 2 mm spaced grid under the mouse. The reconstructed mesh which conforms to the animal external boundary corresponds to a volume of 5.0 cm^3 with 2310 nodes with a nominal sampling rate of 2 mm in x and y and 1 mm in z. The optical heterogeneity map and the fluorescence yield were reconstructed thanks to the method described above (section 3.2).

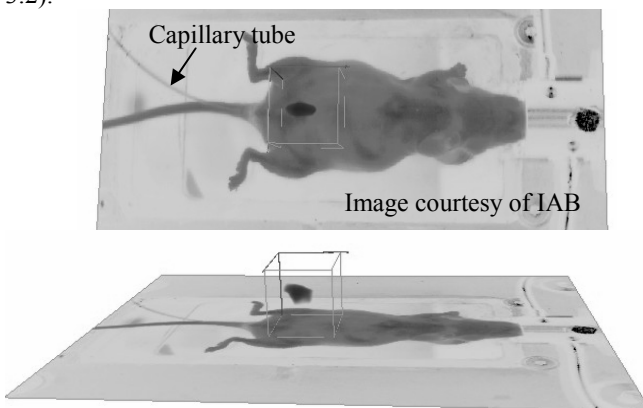


Figure 6: Reconstruction of the capillary tube fluorescence superimposed with the image of the mouse. Two views are displayed to better see the reconstruction in 3D.

We represented the fluorescence yield on Figure 6 where a fluorescent segment can be observed at an anatomically satisfactory position (x,y position as represented in Figure 6 top and a z position found at 1cm for a total mouse thickness of 2cm Figure 6 bottom).

6. CONCLUSION

The method we developed to perform in vivo fDOT reconstruction on an arbitrary shaped small animal was

presented. The system was validated on a cylinder phantom and a nude mouse having a capillary tube filled with Alexa 750 probe. The results are encouraging and validate the performances of our system and its dedicated reconstruction methodology for the study of small animals.

Further experiments will be done on mice bearing mammary murine tumors as the longitudinal study previously conducted with the mouse maintained between two glass plates [8] and results will be compared.

7. ACKNOWLEDGMENT

The authors would like to acknowledge J.L. Coll from INSERM U578 (Institute Albert Bonniot, Grenoble, France) and V. Josserand from ANIMAGE (Bron, France) for having provided, prepared and carried out the mouse experiments.

8. REFERENCES

- [1] D. Boturyn, J.L. Coll, E. Garanger, M.C. Favrot, P. Dumy, "Template assembled cyclopeptides as multimeric system for integrin targeting and endocytosis", *J Am Chem Soc*, 126(18), pp. 5730-9, May 2004.
- [2] Z.H. Jin, J. Razkin, V. Josserand, D. Boturyn, A. Grichine, I. Texier, M.C. Favrot, P. Dumy, J.L. Coll. "In Vivo Noninvasive Optical Imaging of Receptor-Mediated RGD Internalization Using Self-Quenched Cy5-Labeled RAFT-c-(RGDfK-)(4)". *Mol Imaging*. 6(1) pp. 43-55, Jan-Mar2007
- [3] E.E. Graves, J. Ripoll, R. Weissleder, V. Ntziachristos, "A submillimeter resolution fluorescence molecular imaging system for small animal imaging", *Med. Phys.* 30 (5), 901-911 (2003).
- [4] V. Ntziachristos, R. Weissleder, "Experimental three-dimensional fluorescence reconstruction of diffuse media using a normalized Born approximation", *Optics Letters* 26(12), 893-895 (2001).
- [5] V. Ntziachristos, E.A. Schellenberger, J. Ripoll, D. Yessayan, E. Graves, A. Bogdanov, L. Josephson, R. Weissleder, "Visualization of antitumor treatment by means of fluorescence molecular tomography with an annexin V-Cy5.5 conjugate", *P.N.A.S.* 101(33), 12294-12299 (2004).
- [6] L. Hervé, A. Koenig, A. Da Silva, M. Berger, J. Boutet, J. M. Dinten, P. Peltié, and P. Rizo, "Noncontact fluorescence diffuse optical tomography of heterogeneous media," *Appl. Opt.* 46, pp. 4896-4906 (2007).
- [7] S R Arridge and W R B Lionheart. Non-uniqueness in optical tomography *Opt. Lett.* 23 Iss 11, pp. 882-4, 1998.
- [8] A. Koenig et al., fDOT for in vivo follow-up of tumour development in mice lungs. *Proceedings of SPIE, Volume 6629, Diffuse Optical Imaging of Tissue*, Brian W. Pogue, Rinaldo Cubeddu, Editors, 662915 (Jul. 6, 2007).